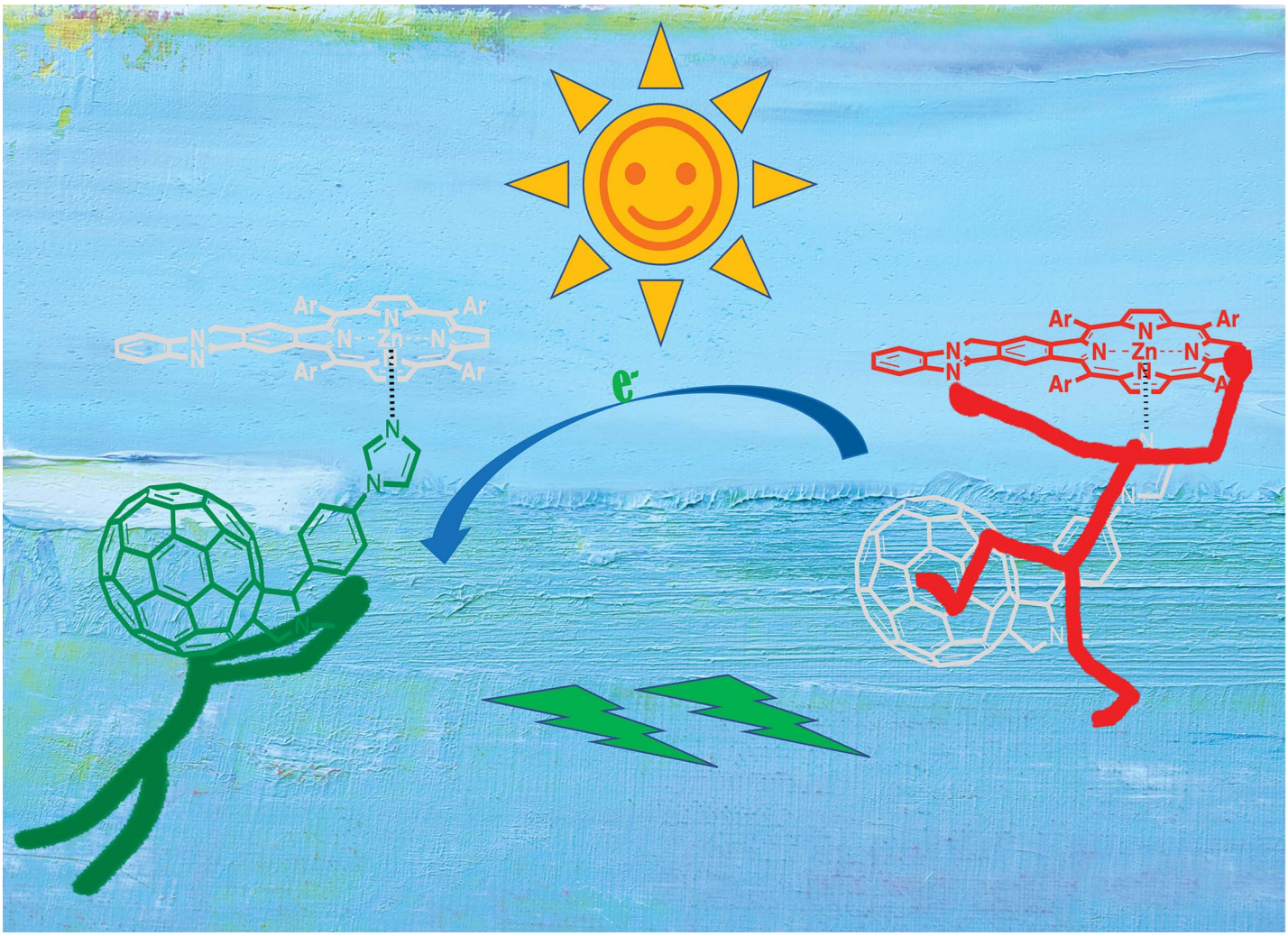

Showcasing research from Professor Wang and D'Souza laboratories, Department of Chemistry, University of North Texas, Denton, TX, United States.

Aromatic heterobicycle-fused porphyrins: impact on aromaticity and excited state electron transfer leading to long-lived charge separation

Aromatic Heterobicycle-Fused Porphyrins were newly designed and synthesized as p-extended UV-visible absorbers. Excited state species of the extended porphyrins were characterized through time-resolved emission and transient absorption spectroscopy. A long-lived photoinduced charge-separated state was observed with fullerene C_{60}-extended porphyrin conjugate. The exceptionally long-lived charge-separated state was attributed to the involvement of both the singlet and the triplet excited states. The availability of this novel highly π-extended structure provides new knowledge and an opportunity to design new organic materials for organic electronics and energy harvesting applications.

As featured in:

See Francis D'Souza, Hong Wang *et al.*, *Chem. Sci.*, 2022, **13**, 9880.

ROYAL SOCIETY OF CHEMISTRY

rsc.li/chemical-science

Registered charity number: 207890

Chemical Science

ROYAL SOCIETY OF CHEMISTRY

EDGE ARTICLE

View Article Online
View Journal | View Issue

Cite this: *Chem. Sci.*, 2022, **13**, 9880

All publication charges for this article have been paid for by the Royal Society of Chemistry

Aromatic heterobicycle-fused porphyrins: impact on aromaticity and excited state electron transfer leading to long-lived charge separation†

Austen Moss,‡ Youngwoo Jang,‡ Jacob Arvidson, Vladimir N. Nesterov, Francis D'Souza * and Hong Wang *

Received 9th June 2022
Accepted 11th August 2022

DOI: 10.1039/d2sc03238d

rsc.li/chemical-science

A new synthetic method to fuse benzo[4,5]imidazo[2,1-*a*]isoindole to the porphyrin periphery at the β,β-positions has been developed, and its impact on the aromaticity and electronic structures is investigated. Reactivity investigation of the fused benzoimidazo-isoindole component reveals fluorescence quenching of a zinc porphyrin (**AMIm-2**) upon treatment with a Brønsted acid. The reaction of the zinc porphyrin (**AMIm-2**) with methyl iodide initiated a new organic transformation, resulting in the ring-opening of isoindole with the formation of an aldehyde and dimethylation of the benzoimidazo component. The fused benzoimidazo-isoindole component acted as a good ligand to bind platinum(II), forming novel homobimetallic and heterobimetallic porphyrin complexes. The fusion of benzoimidazo-isoindole on the porphyrin ring resulted in bathochromically shifted absorptions and emissions, reflecting the extended conjugation of the porphyrin π-system. Time-resolved emission and transient absorption spectroscopy revealed stable excited state species of the benzoimidazo-isoindole fused porphyrins. Zinc porphyrin **AMIm-2** promoted excited state electron transfer upon coordinating with an electron acceptor, C_{60}, generating a long-lived charge-separated state, in the order of 37.4 μs. The formation of the exceptionally long-lived charge-separated state is attributed to the involvement of both singlet and triplet excited states of **AMIm-2**, which is rarely reported in porphyrins.

Introduction

Highly π-extended carbon-rich materials represent fascinating yet challenging frontiers in chemistry and materials science as they offer numerous opportunities in molecular electronics.[1–5] Incorporation of heteroatom(s) into highly π-extended structures can provide control of the electronic structure, and has become a critical strategy to manipulate the materials in order to endow them with desirable properties, such as electrochemical activity, optical absorption spectra, photoluminescence, redox behaviour, charge transfer, bandgap tuning, and other characteristics.[6–9] The development of new methods to introduce heteroatoms or heterocycles is very important to facilitate the growth of this field. Electron delocalization is an important phenomenon in any highly π-conjugated systems. Understanding how the incorporated heteroatoms/heterocycles affect the conjugated systems is of paramount importance to advancing the field.

Porphyrins are aromatic macrocycles, which are nature-selected pigments playing major roles in important biological activities. Due to their unique electronic and photophysical properties, porphyrins have been extensively used in various applications ranging from organic electronics to biomedicines. In recent years, porphyrins have been proven to be effective building blocks in self-assembled materials such as covalent organic frameworks (COFs), metal–organic frameworks (MOFs), and others.[10–18] In this regard, highly π-extended systems obtained through fusing porphyrins with aromatic rings such as polycyclic aromatic hydrocarbons (PAHs) are especially attractive as they are reminiscent of "nanographene" doped with heteroatoms.[1,2,19–42] Theoretically, the fusion of aromatic moieties to the porphyrin periphery can be realized at the *meso*, β- and β,β-positions (Fig. 1). Although synthetically challenging, PAH-fused porphyrins have been achieved through fusion at the *meso*, β-, and β,β-positions.[1,2,19–42] In contrast, the π-extension of porphyrins through the incorporation of aromatic heterocycles is rare and is synthetically more challenging. Only two types of aromatic heterocycles have been used to extend the porphyrin π-conjugated system: pyrazine[43–50] and imidazole[51,52] (Fig. 1). Since the successful development of the synthetic method by Crossley and co-workers in 1991,[48] the pyrazine approach has been widely used in constructing many organic materials for various fundamental studies and applications.[43–50,53,54] Given the

Department of Chemistry, University of North Texas, 1155 Union Circle, #305070, Denton, TX 76203-5017, USA. E-mail: francis.dsouza@unt.edu; hong.wang@unt.edu

† Electronic supplementary information (ESI) available. CCDC 2172827–2172829. For ESI and crystallographic data in CIF or other electronic format see https://doi.org/10.1039/d2sc03238d

‡ Equal contribution.

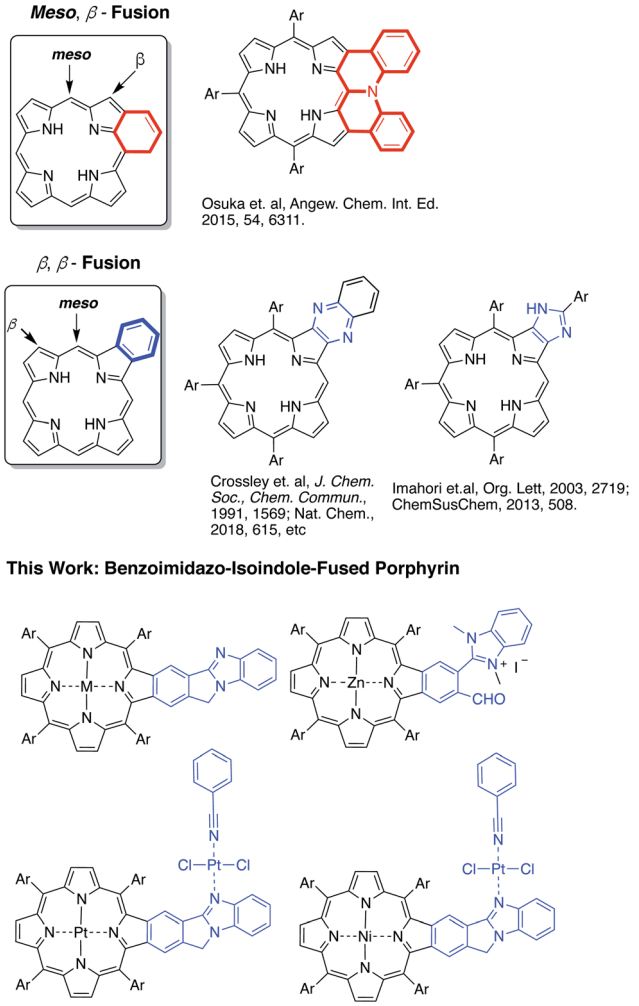

Fig. 1 Structures of the benzoimidazo-isoindole-fused porphyrins.

ubiquitous roles aromatic heterocycles play in organic materials science, it is important to develop new strategies to incorporate aromatic heterocycles into highly π-extended structures.

In this work, a new synthetic method was developed to fuse benzo[4,5]imidazo[2,1-*a*]isoindole to porphyrins at the porphyrin β,β-positions (Fig. 1).[55] The benzimidazole moiety has been widely used in drug development.[56,57] Benzimidazole is also known to serve as a ligand to metals.[58–60] However, the impact of the benzimidazole moiety on aromaticity and electronic structures of π-extended structures remains elusive. Benzo[4,5]imidazo[2,1-*a*]isoindole induces intrinsic dipole moments in the π-extended molecule owing to the presence of the amidine component (Fig. 1) and is expected to bring in new features. The newly synthesized benzo[4,5]imidazo[2,1-*a*]isoindole-fused porphyrins have been studied using spectral, electrochemical, DFT, and time-resolved emission and transient absorption spectral methods to probe the effect of benzoimidazo-isoindole fusion on the overall physico-chemical properties. The ability of this class of compounds to promote excited-state electron transfer has also been investigated using zinc porphyrin **AMIm-2** as an electron donor and fullerene C_{60} as an electron acceptor. Our studies show that both the singlet and triplet excited states of **AMIm-2** were involved in the electron transfer process, yielding a long-lived charge-separated state of the order of 35 μs.

Results and discussion

Molecular design and synthesis

The synthetic methods developed in our group for π-extended porphyrins open the door to functionalizing π-extended porphyrins at porphyrin β,β-positions.[61–65] Our initial plan was to synthesize a phthalaldehyde-fused porphyrin (**1**, Scheme 1) that would react with *o*-phenylenediamine to form a 1,4-diazocine-fused porphyrin, which is "non-aromatic" in the ground state, in order to study the interaction between the heteroatom-containing diazocine and porphyrin (Scheme 1). To our surprise, the reaction between the monobenzoporphyrin (**1**) and *o*-phenylenediamine under acidic conditions (*p*-TsOH/dichloromethane (DCM)) did not yield the desired 1,4-diazocine-fused porphyrin. Instead, a complex mixture resulted. After careful analysis of this mixture, we were able to isolate a new porphyrin, which was identified as a benzo[4,5]imidazo[2,1-*a*]isoindole-fused porphyrin (**AMIm-1**) (Scheme 1). This exciting result prompted us to scrutinize the literature and we found that Chen, J. *et al.* reported a similar method to synthesize benzo[4,5]imidazo[2,1-*a*]isoindoles.[55] We then optimized Chen's original procedure (HCOOH/MeOH) to develop suitable conditions for porphyrins. Changing the solvent from MeOH to dichloromethane (DCM) and raising the temperature from 0 °C to room temperature significantly increased the efficacy of this reaction, affording **AMIm-1** in 80% yield. Due to the immiscibility of the dichloromethane and the 88% formic acid used in the reaction, the reaction is biphasic, which led to easy separation and purification of the product. This methodology is high-yielding and extremely concise as it does not require lengthy purification protocols using column chromatography. Subsequent insertion of zinc(II) into the porphyrin core afforded **AMIm-2** in 92% yield (see the ESI for synthetic details and Fig. S1 and S2† for ^{1}H NMR and FT-IR spectra).

Activity of the fused benzo[4,5]imidazo[2,1-*a*]isoindole

Benzo[4,5]imidazo[2,1-*a*]isoindole induces intrinsic dipole moments as shown in Scheme 2. Benzo[4,5]imidazo[2,1-*a*]

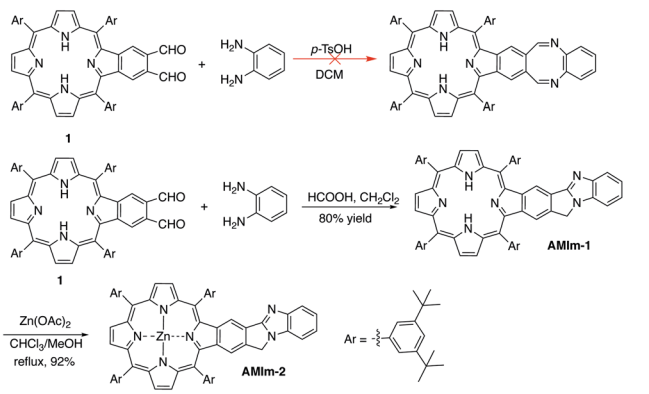

Scheme 1 Synthesis of benzo[4,5]imidazo[2,1-*a*]isoindole-fused porphyrins.

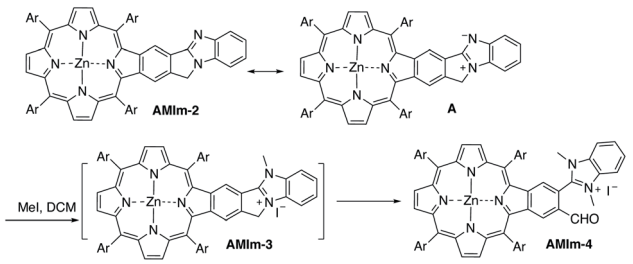

Scheme 2 Resonance structure and reactivity of AMIm-2 with methyl iodide.

isoindole can be treated as isoindole fused with benzimidazole. If the resonance structure **A** (Scheme 2) can be trapped, it will provide these porphyrins with new features and opportunities. Methylation of the more basic nitrogen of the amidine appeared to be a plausible approach. We decided to treat **AMIm-2** with excess MeI (0.2 ml) in DCM (1 ml). The reaction was tracked with UV-vis spectroscopy. Changes started to appear after one day and the reaction was stopped until no further changes were observed after three days. The product was isolated through recrystallization in DCM/MeOH. To our surprise, the ^{1}H NMR spectra of this product displayed a completely different pattern from that of **AMIm-2** showing an aldehyde peak at 9.75 ppm, which did not match the expected **AMIm-3**. The nature of this reaction remained a mystery until the crystal structure of this product was resolved (see ESI Fig. S3 for the structure and ESI Table S1 for the crystallographic data, CCDC: 2172828†). The crystal structure of **AMIm-4** reveals that methylation occurred to both nitrogen atoms on the imidazole ring, and the 5-membered ring of the isoindole component was cleaved leaving a hanging methylated imidazole group and an aldehyde group. This organic transformation reaction has not been reported in the literature. The mechanism remains elusive. Cleavage of the C–N bond may be plausible given that the nitrogen carries a positive charge. However, the conversion to a carbonyl group was not understood, but could be related to the minor amount of H_2O present in the reaction mixture and needs further investigation.

Benzimidazole is a base. It can also serve as a ligand to metals. However, this benzimidazole component is fused in the system and thus has no rotational flexibility. It will be interesting to explore its binding ability as it can potentially provide two metal-binding sites within the highly π-extended system (Scheme 3). **AMIm-1** was treated with $Zn(OAc)_2$ and $Ni(OAc)_2$ under respective metal insertion conditions, and metalation of the porphyrin core was observed for both metals, affording the corresponding metalated products (**AMIm-2** and **AMIm-5**) (Scheme 3). However, binding to the benzimidazole site was not observed in both cases. We then attempted to metalate **AMIm-1** with $PtCl_2$ as platinum porphyrins/complexes are of broad interest in various areas.[66–70] **AMIm-1** was treated with $PtCl_2$ in benzonitrile under reflux. To our surprise, Pt(II) was able to bind both at the porphyrin core and at the imidazole site, affording the homo-bimetallic complex **AMIm-6** in a 56% yield. Encouraged by this result, **AMIm-2** and **AMIm-5** were subjected to

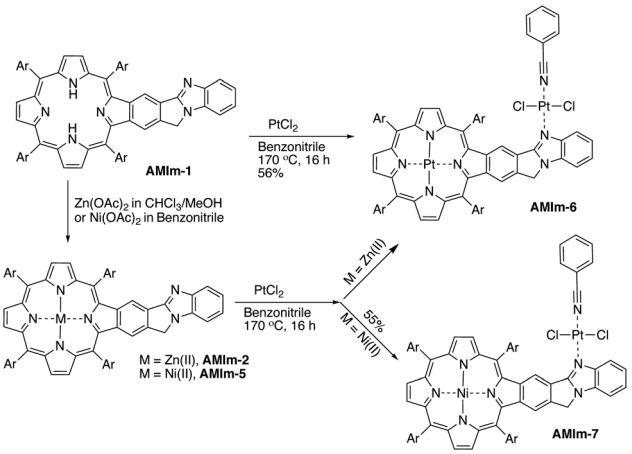

Scheme 3 Reactivity of AMIm-1 with different metal ions and the resulting products.

reactions with platinum chloride in benzonitrile respectively to obtain heterobimetallic complexes. Heterobimetallic **AMIm-7** was successfully obtained with **AMIm-5**. However, the reaction of $PtCl_2$ with **AMIm-2** resulted in an inseparable mixture with the homometallic **AMIm-6** identified as the major product. Apparently, Zn(II) was kicked out of **AMIm-2** and Pt(II) was inserted at both binding sites.

Crystal structures

The single crystal structure of **AMIm-6** (CCDC: 2172827†) and **AMIm-7** (CCDC: 2172829, see Tables S2 and S3† for structural parameters) was obtained (Fig. 2). In **AMIm-6**, the Pt(II) porphyrin ring and the fused benzo[4,5]imidazo[2,1-*a*]isoindole unit stay essentially in the same plane. The second Pt(II) is bonded to two chloride groups, the imidazole nitrogen, and a benzonitrile molecule which came from the solvent for the platinum insertion reaction. The second Pt(II) has a typical square planar geometry and is assumedly locked perpendicular to the porphyrin plane likely due to steric interaction of the neighbouring di-*tert*-butylphenyl group. In **AMIm-7**, the

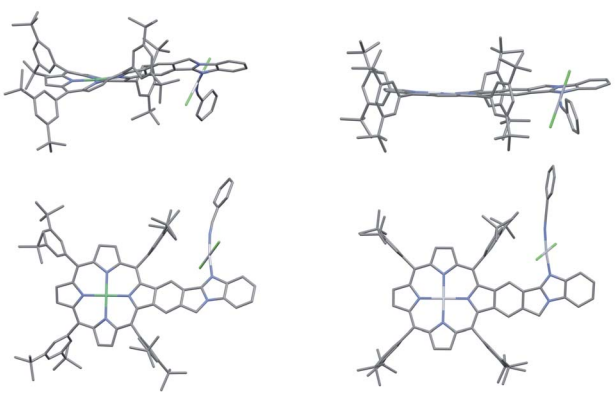

Fig. 2 X-ray crystal structures of AMIm-6 (right) and AMIm-7 (left). Top: top view. Bottom: side view. All hydrogen atoms are omitted for clarity.

coordination sphere of Pt(II) is similar to that of **AMIm-6**, adopting a square planar geometry, which is perpendicular to the porphyrin ring. The porphyrin ring of **AMIm-7** is distorted due to the presence of Ni(II). These structures provide direct evidence for the involvement of the benzimidazole functionality in metal binding.

Spectral, computational and electrochemical studies

Having established the synthesis, structure, and reactivity of the benzoimidazo-isoindole-fused porphyrins, systematic studies were then performed to evaluate the effect of benzoimidazo-isoindole-fusion on the spectral, electrochemical, and photochemical properties of these novel π-extended porphyrins.

Absorption and emission spectroscopy. The UV-vis absorption spectra of **AMIm-1**, **AMIm-2**, and **AMIm-5–AMIm-7** in toluene are compiled in Fig. 3a. The free-base **AMIm-1** displayed an intense Soret band centered at 435 nm. Upon metal insertion of zinc and nickel, the Soret bands were red-shifted to 442 nm (**AMIm-2**) and 437 nm (**AMIm-5**). All these porphyrins showed the expected number of Q-bands, *viz.*, **AMIm-2** and **AMIm-5** with two Q-bands, and **AMIm-1** showing four Q-bands. On the other hand, the bimetallic platinum porphyrin (**AMIm-6**) showed a very blue-shifted Soret band at 426 nm as compared with free base **AMIm-1**. In contrast, the Soret band of the hetero-bimetallic **AMIm-7** was red-shifted by 17 nm relative to that of homobimetallic **AMIm-6**. The two Q bands of **AMIm-6** displayed a similar trend. Titration of **AMIm-2** with trifluoroacetic acid displayed a clear red-shift and significant intensity decrease of the Soret band (see ESI Fig. S4 and S5† for absorption and fluorescence spectral changes during acid titration). These data suggest the conjugation of the porphyrin with the fused benzoimidazo-isoindole component. The luminescence spectra for **AMIm-1** and **AMIm-2** along with their singlet lifetimes were recorded (Fig. 3b). Free-base **AMIm-1** has an emission band centered around 660 nm (Stokes shift of 8 nm) and another emission band centered around 726 nm. The fluorescence lifetime of **AMIm-1** was 13.6 ns, which was typical for free-base porphyrins. The fluorescence emission peaks of **AMIm-2** appeared at 604 and 664 nm with a lifetime of about 2 ns, close to that of zinc porphyrins. Phosphorescence of **AMIm-2** was also recorded at liquid nitrogen temperature. The phosphorescence maximum was located at 855 nm (Fig. 3b). From these spectral data, the singlet–singlet energy, $E_{0,0}$, and triplet energy, E_T, were evaluated. The $E_{0,0}$ values for **AMIm-1** and **AMIm-2** were found to be 1.97 and 2.05 eV, respectively, and the E_T value for **AMIm-2** was found to be 1.45 eV. Platinum complex **AMIm-6** displayed no fluorescence but only phosphorescence due to the large heavy metal effect of two platinum atoms promoting inter-system crossing to the triplet state with an emission band at 677 nm (see the ESI†). It is interesting to note that acid titration of **AMIm-2** showed fluorescence quenching (see Fig. S2 in the ESI†), which has potential application in oxygen sensing.[71,72]

DFT calculations. Structures of **AMIm-1**, **AMIm-2**, **AMIm-6**, and a tautomer of **AMIm-1** (**AMIm-1′**) were optimized using B3LYP functional and 6-31G(d,p) basis set for all atoms besides platinum, and basis set LANL2DZ for the platinum atoms in **AMIm-6**.[73–77] The calculated isodensity surfaces for

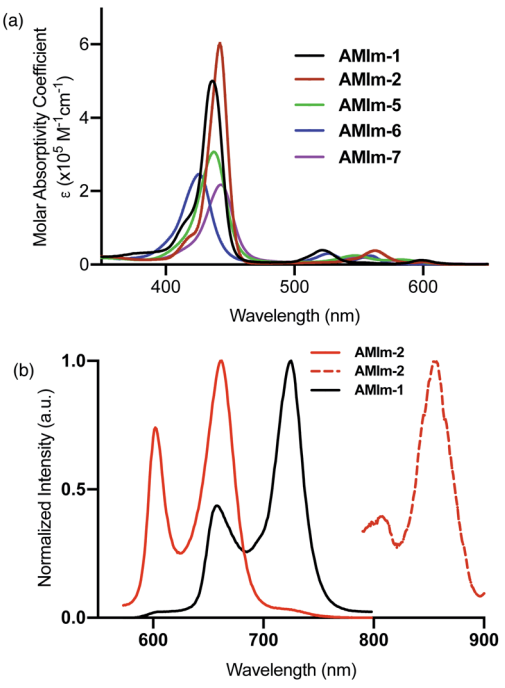

Fig. 3 (a) Absorption and (b) normalized fluorescence and phosphorescence spectra of the indicated compounds in dichlorobenzene (DCB).

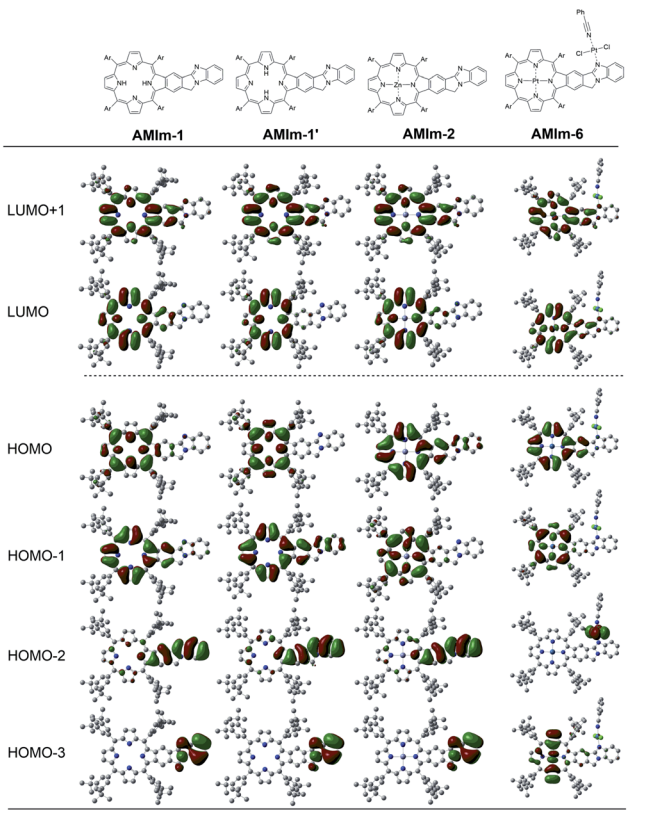

Fig. 4 B3LYP/6-31G* optimized structures and frontier orbitals of the indicated molecular systems.

benzimidazole-fused porphyrins are shown in Fig. 4. Analysis of the molecular orbitals and energy level diagram (see Fig. S6–S10 in the ESI† for optimized structures, frontier orbital energies, and calculated spectra, and Tables S4–S8 for oscillator strength values and coordinates of optimized structures) indicates that the monomers largely align with Gouterman's 4-orbital model[78,79] in that the HOMO−1/HOMO and LUMO/LUMO+1 are respectively almost degenerate. However, **AMIm-6** shows states that are closer in energy to the HOMO and LUMO. As the HOMO−2 of **AMIm-6** has electron density exclusively around the benzimidazole bound platinum complex, it is possible that the external platinum complex plays a significant role in the electronic transitions of **AMIm-6**. It is notable that while there is substantial electron density on the benzimidazole component in HOMO−3 and HOMO−2 of **AMIm-1**, **AMIm-1′**, and **AMIm-2**, there is no electron density on the porphyrin in these isodensity surfaces. This observation indicates that the benzimidazole and porphyrin might act more as independent chromophores than as a fused multichromophoric system. In contrast, there is electron density present across the sp^3 hybridized C–H bonds between the porphyrin and benzimidazole in the HOMO−3 and LUMO+1. Such electron density distribution indicates homo-conjugated characteristics[80–82] across the sp^3 hybridized CH_2 bonds that bridge the benzimidazole and porphyrin, which could explain the significant red-shifting of the absorption bands upon acid titration of **AMIm-2** and binding of Pt(II) in **AMIm-7**. In the case of **AMIm-6**, this is only observed in the LUMO+1 and not in the HOMO−3. We also performed TD-DFT calculations using B3LYP and basis set 6-31G(d,p) with an IEFPCM solvation model in toluene to understand the nature of the electronic transitions in these molecules. The obtained oscillator strengths are overlayed with the experimental UV-vis for each molecule (see the ESI†) and appear to be in agreement. The calculation data and interpretations are included in the ESI.†

Electrochemistry. The electrochemical redox behaviour of both **AMIm-1** and **AMIm-2** was evaluated using differential pulse voltammetry in DCB containing 0.1 M $(TBA)ClO_4$ and is displayed in Fig. 5. Within the accessible potential window, both compounds revealed two one-electron reductions and up to three one-electron oxidations. For **AMIm-1**, reductions at −1.96 and −1.74 V, and oxidations at 0.50, 0.60 and 0.88 V *vs.* Fc/Fc^+ were observed. Similarly, for **AMIm-2**, reductions at −2.12 and −1.91 V, and oxidations at 0.19, 0.40 and 0.87 V *vs.* Fc/Fc^+ were observed. The appearance of a third oxidation in both molecules instead of the traditionally observed two one-electron oxidations of both free-base and zinc porphyrins[83] suggests the likely involvement of the fused benzoimidazo-isoindole in subsequent oxidation processes.

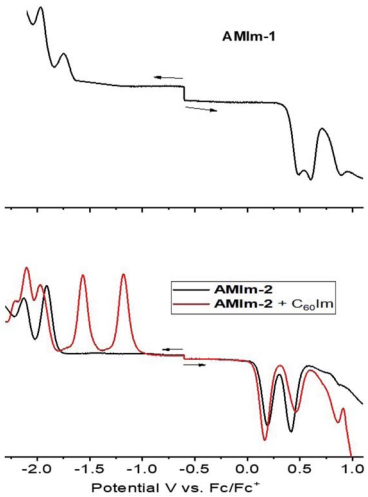

Fig. 5 Differential pulse voltammograms of the indicated molecular systems in DCB containing 0.1 M $(TBA)ClO_4$.

Photochemical properties

The excellent spectral and redox properties of **AMIm-1** and **AMIm-2** further prompted us to investigate their photophysical properties along with their ability to undergo excited-state electron transfer reactions. With this in mind, first, the transient spectral behaviour of both compounds was investigated using femtosecond- (fs-TA) and nanosecond transient absorption (ns-TA) techniques. The former technique probes mainly photo-events originating from the singlet excited state while the latter probes events from the triplet excited state.

Fig. 6a shows the fs-TA spectra of **AMIm-1** at the indicated delay times. At the Soret band excitation, the excited S_2 state populated the S_1 state within the first ps *via* the process of internal conversion (IC). The S_1 state revealed excited state absorption peaks at 457, 550, 623, 749, 1125, and 1293 nm. This was accompanied by negative peaks at 518, 595, 660, and 722 nm. By comparison with the earlier discussed absorption and fluorescence, it could be deduced that the first two peaks corresponded to the process of ground-state bleaching (GSB) and the latter two to the stimulated emission (SE) process. The decay of the ESA peaks and the recovery of the SE and GSB peaks were rather slow, consistent with the long lifetime of ^{1}**AMIm-1*** of 13.6 ns (see the Fig. 6a inset for the decay profile of the 1120 nm peak). Ns-TA spectra were also subsequently recorded to characterize the ^{3}**AMIm-1*** formed *via* the process of inter-system crossing (ISC) of ^{1}**AMIm-1***. Triplet–triplet absorption peaks of ^{3}**AMIm-1*** were located at 455, 559, 628, and 918 nm. From the decay profile of the 455 nm band (see the Fig. 6b inset) a lifetime of 34.65 μs was obtained.

The fs-TA spectra of ^{1}**AMIm-2*** at the indicated delay times are shown in Fig. 6c. The S_1 state formed from the rapid internal conversion of the S_2 state revealed ESA peaks at 478, 585, 621, 692, 988, and 1194 nm. This was accompanied by negative peaks at 558, 604, and 667 nm. By spectral comparison, it could be deduced that among these peaks, the first two corresponded to GSB and part of the second and third peaks to SE. Decay of the positive peaks and recovery of the negative peaks were relatively fast (see the Fig. 6c inset for the decay profile of the 1194 nm peak), consistent with the short lifetime of ^{1}**AMIm-2*** of 2 ns. Subsequent ns-TA, shown in Fig. 6d, revealed peaks corresponding to ^{3}**AMIm-2*** at 440, 624, 769, and 1013 nm. By monitoring the decay profile of the 470 nm peak (see the Fig. 6d inset), a lifetime of 82.42 μs was obtained.

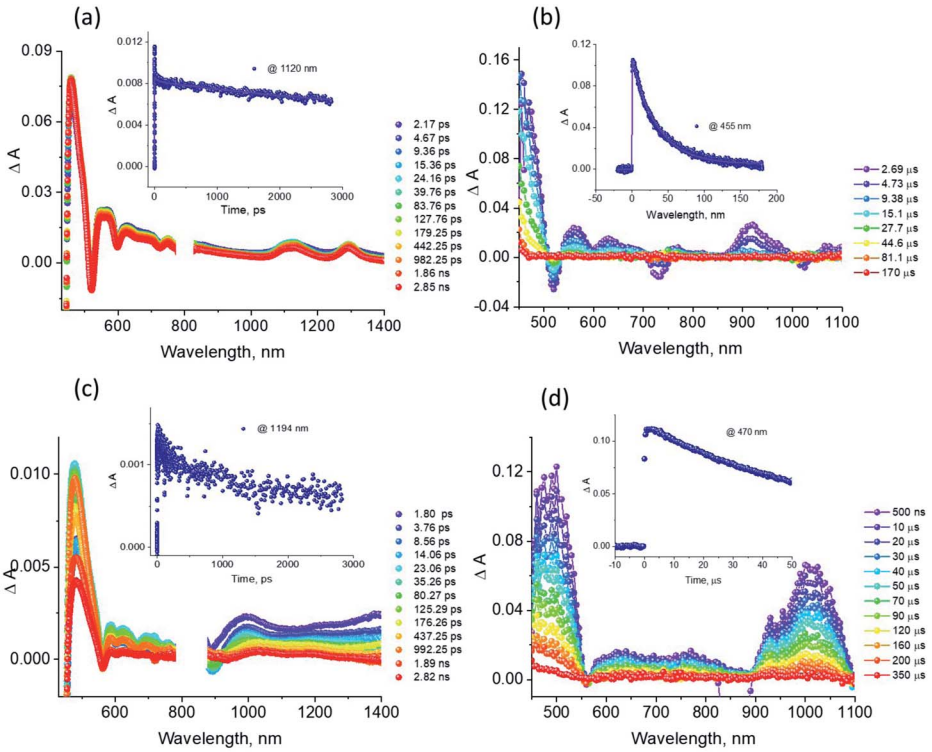

Fig. 6 (a and c) Femtosecond transient absorption spectra at the indicated delay times, and (b and d) nanosecond transient absorption spectra of (a and b) **AMIm-1** and (c and d) **AMIm-2** in DCB. The samples were excited at their corresponding Soret band maxima. The decay profiles at the indicated wavelengths are shown in the figure inset.

Light-induced electron transfer

The physico-chemical properties along with the excited state features of the benzoimidazo-isoindole-fused porphyrins further prompted us to use them as electron donors in excited state electron transfer reactions. The zinc derivative **AMIm-2** was utilized in this case study owing to its facile oxidation, favorable $E_{0,0}$ and E_T values, and well-behaved singlet and triplet transient spectral features. With regard to the electron acceptor, the well-known electron acceptor fullerene C_{60}[84] has been employed using a self-assembly approach of metal–ligand axial coordination. For this, C_{60} is functionalized with an axially coordinated ligand, phenyl imidazole, C_{60}Im.[85]

The coordinatively unsaturated zinc in zinc porphyrins is known to bind nitrogenous ligands with moderate stability.[85,86] This also seems to be the case in **AMIm-2**. As shown in Fig. 7a, the increased addition of C_{60}Im to a solution of **AMIm-2** in DCB revealed the diminished intensity of the Soret and visible bands with redshifts. Isosbestic points at 410, 455, and 569 nm were observed indicating the existence of an equilibrium. The equilibrium constant, K, evaluated using the Benesi–Hildebrand method[86] was found to be 7.2×10^4 M^{-1} (see the Fig. 7a inset for the plot) suggesting moderate stability. The linear plot also suggests 1 : 1 stoichiometry. The fluorescence spectrum of **AMIm-2** was also recorded during the process of titration, as shown in Fig. 7b. Both bands revealed quenching over 80% indicating the occurrence of excited state photo-events such as electron or energy transfer.[86] It may be mentioned here that when the **AMIm-2:ImC$_{60}$** complex was excited either at the Soret (Fig. 7b) or visible band maxima, no emission around 715 nm corresponding to C_{60}Im was observed, thus ruling out the possibility of energy transfer as the quenching mechanism or indicating that such a process is a minor one in the donor–acceptor dyad.

The B3LYP/6-31G* optimized structures and frontier orbitals of the **AMIm-2:ImC$_{60}$** complex (see Fig. S11 in the ESI†) clearly reveal the formation of a 1 : 1 complex without any steric constraints. Interestingly, the LUMO confined to the **AMIm-2** macrocycle (see Fig. S11 in the ESI†) is now on C_{60} establishing the latter's role as an electron acceptor. The majority of the HOMO was on the porphyrin π-structure while HOMO−1 was extended to the benzoimidazole part of the molecule suggesting π-extension also in the oxidized form of **AMIm-2**.

The electrochemical studies also helped in realizing the metal–ligand binding induced redox changes and facile reduction of C_{60} compared to that of the zinc porphyrin in the **AMIm-2:ImC$_{60}$** complex, as shown in Fig. 5. Coordination of C_{60}Im cathodically shifted the oxidation peak of **AMIm-2** by 30 mV at 0.16 V *vs.* Fc/Fc^+ and the reduction peak by 60 mV at −1.97 V. The first two reductions of C_{60}Im were located at −1.17 and −1.55 V (see the red trace in the lower panel of Fig. 5).

An energy diagram was subsequently established to visualize the electron transfer reaction (Fig. 8). The energy of the excited states was calculated from the earlier discussed spectral data while that of the charge-separated state was calculated using redox data according to the Rehm–Weller approach.[87] The

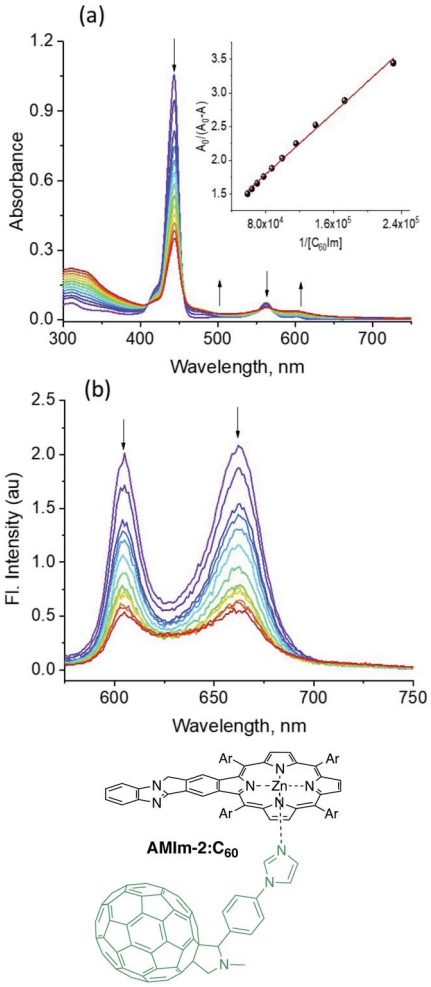

Fig. 7 (a) Absorption and (b) fluorescence spectral changes of AMIm-2 on increasing addition of C_{60}Im. The Benesi–Hildebrand plot to evaluate the binding constant is shown in the inset of (a). The sample was excited at the Soret band peak maximum.

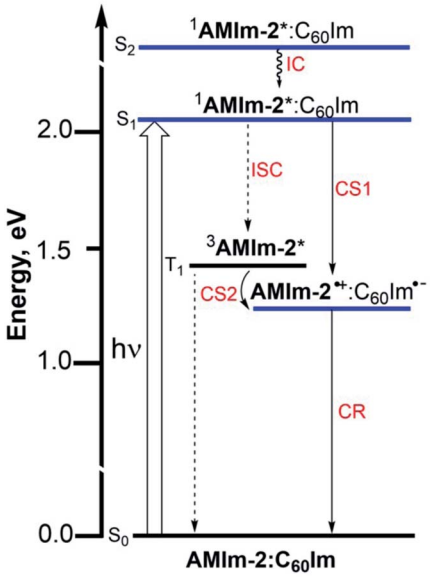

Fig. 8 Energy level diagram showing photoinduced electron transfer originating from both singlet and triplet excited states of AMIm-2 in the presence of coordinated C_{60}Im.

thermodynamic feasibility of excited electron transfer from both the singlet and triplet excited states of **AMIm-2** is obvious from the energy diagram, with $-\Delta G^{S}_{CS} = 0.83$ eV and $-\Delta G^{T}_{CS} = 0.22$ eV. The energy of the charge-separated state which equals the free-energy change for charge recombination ($-\Delta G_{CR}$) is relatively high, being about 1.23 eV (this also assumes the energy of the singlet and triplet radical ion-pairs to be almost the same). Under such circumstances, the charge recombination could fall in the inverted region of the Marcus parabola[88] potentially extending the lifetime of the charge-separated state. In addition, if electron transfer also occurs from the ^{3}**AMIm-2*** state, then one would expect a long-lived charge-separated state due to different spins of the radical ion-pair. To secure evidence of triplet quenching, the phosphorescence spectrum of **AMIm-2** was recorded in the presence of C_{60}Im at liquid nitrogen temperature, as shown in Fig. S12 in the ESI.† Quenching of phosphorescence was observed (over 80%) indicating the occurrence of photochemical events from the triplet excited state. It may also be pointed out here that since the spectrum was recorded at liquid nitrogen temperature, it is safe to conclude that the quenching process is intramolecular involving the **AMIm-2:ImC$_{60}$** complex, and not intermolecular as no diffusion of donor and acceptor entities could be expected in the frozen state. Systematic transient absorption spectral studies were performed using both fs-TA and ns-TA techniques to characterize the electron transfer events from the singlet and triplet excited states and to determine the kinetics of these photo-events.

Fig. 9a compares the fs-TA spectra of **AMIm-2** and **AMIm-2:ImC$_{60}$** complex in dichlorobenzene (DCB) at a delay time of 242 ps. Complete fs-TA spectra of **AMIm-2:ImC$_{60}$** at different delay times are shown in Fig. S13a in the ESI.† The presence of **ImC$_{60}$** deactivated the ESA and GSB/SE peaks of **AMIm-2** much more rapidly accompanied by the appearance of new peaks in the visible region at 644 and 690 nm and a near-IR peak in the 1000 nm region.

Chemical oxidation of **AMIm-2** confirmed that the visible bands are due to the formation of **AMIm-2$^{\bullet+}$** while the near-IR peak is due to the formation of **ImC$_{60}^{\bullet-}$** (see the dashed line in Fig. 9d). These spectral results provide direct proof for the occurrence of electron transfer from the S_1 state of porphyrin in the **AMIm-2:ImC$_{60}$** complex. For the determination of the rate of charge separation from the singlet excited state, k^{S}_{CS}, the decay time constant of the near-IR ESA peak of **AMIm-2** was monitored, as shown in Fig. 9b. Faster decay of this peak in the presence of C_{60}Im can be clearly seen in this plot. From the decay time constants, a value of $k^{S}_{CS} = 3.24 \times 10^{10}$ s^{-1} was obtained. For the determination of the rate of charge recombination of the singlet radical ion-pair, k^{S}_{CR}, the **AMIm-2$^{\bullet+}$** peak at 695 nm was monitored, as shown in Fig. 9c. A k^{S}_{CR} value of 3.52×10^{8} s^{-1} was determined; however, the signal persisted beyond the 3 ns monitoring window of the femtosecond transient setup. Under such conditions, the measured k^{S}_{CR} could be treated as the upper limit.

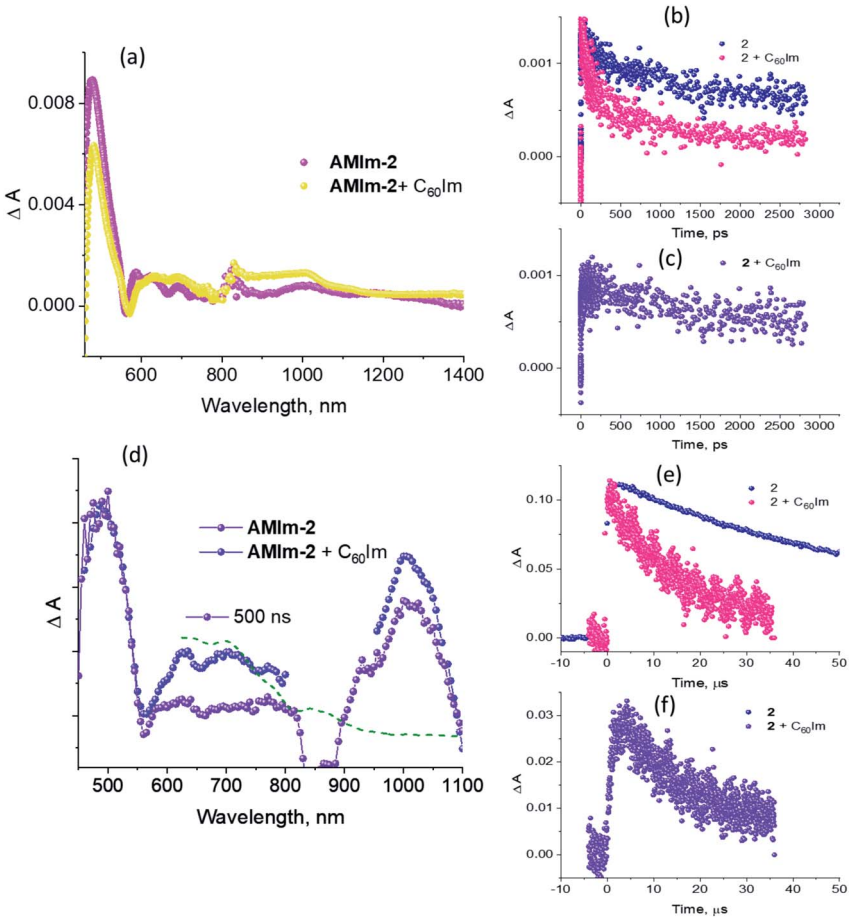

Fig. 9 (a) Fs-TA spectra of **AMIm-2** and **AMIm-2**:ImC_{60} complex in DCB at a delay time of 242 ps and an excitation wavelength of 420 nm. (b) Decay profile of the near-IR ESA peaks. (c) Decay profile of **AMIm-2**$^{\bullet+}$ monitored at 695 nm for the dyad. (d) Nanosecond transient spectra, normalized to the 470 nm peak, of **AMIm-2** and **AMIm-2**:ImC_{60} complex in DCB at a delay time of 500 ns and an excitation wavelength of 420 nm. (e) Decay profile of the 470 nm peak corresponding to ^{3}**AMIm-2***. (f) Decay profile of the **AMIm-2**$^{\bullet+}$ monitored at 690 nm. The dashed line in (d) represents the spectrum of chemically oxidized **AMIm-2** ($NOBF_4$ was used as an oxidizing agent).

Further, ns-TA spectra were also recorded for the **AMIm-2:ImC$_{60}$** complex. Fig. 9d shows the corresponding spectra, normalized to the 470 nm triplet peak, of **AMIm-2** and **AMIm-2:ImC$_{60}$** complex at a delay time of 500 ns in DCB (see Fig. S13b in the ESI† for full spectral features of the complex). Such a spectral comparison was warranted since the spectrum of ^{3}**AMIm-2*** had ESA peaks both in the visible and near-IR regions where radical cation and radical anion peaks were expected. In the presence of C_{60}Im, ^{3}**AMIm-2*** revealed faster decay, similar to that observed for the ^{1}**AMIm-2*** species suggesting its involvement in the electron transfer process (see Fig. 9e for decay curves). Interestingly, the **AMIm-2**$^{\bullet+}$ peaks in the visible region and the $\mathbf{ImC_{60}^{\bullet-}}$ peak in the near-IR region were clearly visible with contributions from ^{3}**AMIm-2***. From the decay curves of ^{3}**AMIm-2*** monitored at 470 nm, a value of $k_{CS}^{T} = 3.24 \times 10^4$ s^{-1} was obtained. Similarly, by monitoring the **AMIm-2**$^{\bullet+}$ peak at 690 nm (see Fig. 9f for the decay curve) a value of $k_{CR}^{T} = 2.68 \times 10^4$ s^{-1} was obtained. From the k_{CR}^{T} value, a lifetime of the charge-separated state of 37.4 μs was obtained, the highest observed for zinc porphyrin–fullerene dyads assembled *via* the metal–ligand axial coordination approach.

Conclusions

This work introduces a novel class of highly π-extended structures with interesting properties through fusing porphyrin with aromatic heterobicycles. A new method has been developed to fuse an aromatic heterobicycle, *i.e.*, benzo[4,5]imidazo[2,1-*a*]isoindole, to the porphyrin periphery. The π-extended porphyrins fused with benzo[4,5]imidazo[2,1-*a*]isoindole displayed unprecedented reactivities toward methyl iodide and platinum(II). A new organic transformation was discovered when **AMIm-2** was treated with MeI, resulting in ring-opening of the fused isoindole component and formation of an aldehyde functional group. Upon treatment with $PtCl_2$, both homobimetallic and heterobimetallic complexes were obtained (**AMIm-6** and **AMIm-7**), offering a new class of metal complexes.

The fusion of heterobicycles to the porphyrin ring results in a bathochromic shift of absorptions for the free base, zinc, and nickel benzoimidazo-isoindole-fused porphyrins (**AMIm-1**, **AMIm-2**, and **AMIm-5**) relative to those of their unfused analogues. On the other hand, while the homobimetallic Pt(II) complex **AMIm-6** displayed a blue-shifted Soret band as

compared with that of **AMIm-1**, **AMIm-2**, and **AMIm-5**, that of the heterobimetallic **AMIm-7** was very red-shifted, reflecting a significant effect on metal ion induced spectral changes. It is notable that zinc porphyrin **AMIm-2** demonstrated fluorescence quenching upon treatment with an acid. In contrast to the experimental spectroscopic data which indicate the conjugation of the heterocycles to the porphyrin π-system, the HOMO and LUMO obtained from DFT calculation showed minimal involvement of the heterocycles. These contradicting data suggest that the traditional Gouterman 4-orbital model[78,79] cannot interpret the observed spectroscopic data, and a more complex model should be developed.

Photoinduced electron transfer properties of the zinc porphyrin derivative, **AMIm-2**, in the presence of C_{60} revealed a long-lived charge-separated state, in the order of 37.4 μs. It is interesting that the intramolecular electron transfer occurred from both the singlet and the triplet excited states. Intramolecular photoinduced electron transfer from the singlet excited state is commonly reported in the literature;[84–86] however, such reactions from the triplet excited state are not common.[89] The exceptionally long-lived charge-separated state observed in this work was attributed to the involvement of the triplet excited state. Stable excited state species of the benzoimidazo-isoindole-fused porphyrins were also identified through time-resolved emission and transient absorption spectroscopy. The availability of this highly π-extended structure provides new knowledge and an opportunity to design and explore new organic materials for organic electronics and energy harvesting.

Data availability

Crystallographic data for **AMIm-4**, **AMIm-6** and **AMIm-7** have been deposited at the Cambridge Crystallographic Data Centre (**AMIm-4**, CCDC: 2172828; **AMIm-6**, CCDC: 2172827, **AMIm-7**, CCDC: 2172829). Experimental procedures, ^{1}H and ^{13}C NMR spectra and computational methods, which support this article, have been uploaded as part of the supplementary material.

Author contributions

H. W. and A. M. designed the project. A. M. and J. A. conducted the synthesis and characterization, and initial spectral studies of the compounds. Y. J. and F. D. designed and carried out the experiments for electrochemical measurement and transient spectroscopy. A. M. and Y. J. performed all the computations. V. N. N. collected the X-ray diffraction data and solved the crystal structures. All authors contributed to data analysis and manuscript writing.

Conflicts of interest

There are no conflicts to declare.

Acknowledgements

This work was supported by the U.S. Department of Energy, Office of Science, Basic Energy Sciences under Award DE-SC0016766. Our gratitude goes out to Dr Guido Verbeck and the Laboratory for Imaging Mass Spectrometry at the University of North Texas for MALDI-Orbitrap Mass Spectrometry data. We acknowledge the National Science Foundation MRI Program (CHE-1726652) and the University of North Texas for supporting the acquisition of the Rigaku XtaLAB Synergy-S X-ray diffractometer.

Notes and references

1 M. Stepien, E. Gonka, M. Zyla and N. Sprutta, *Chem. Rev.*, 2017, **117**, 3479–3716.
2 A. Narita, X. Y. Wang, X. Feng and K. Mullen, *Chem. Soc. Rev.*, 2015, **44**, 6616–6643.
3 I. Pozo, E. Guitian, D. Perez and D. Pena, *Acc. Chem. Res.*, 2019, **52**, 2472–2481.
4 X. Liu, S. Y. Chen, Q. Chen, X. Yao, M. Gelleri, S. Ritz, S. Kumar, C. Cremer, K. Landfester, K. Mullen, S. H. Parekh, A. Narita and M. Bonn, *Angew. Chem., Int. Ed. Engl.*, 2020, **59**, 496–502.
5 E. M. Muzammil, D. Halilovic and M. C. Stuparu, *Commun. Chem.*, 2019, **2**, 58.
6 X. Wang, G. Sun, P. Routh, D. H. Kim, W. Huang and P. Chen, *Chem. Soc. Rev.*, 2014, **43**, 7067–7098.
7 S. Kawai, S. Nakatsuka, T. Hatakeyama, R. Pawlak, T. Meier, J. Tracey, E. Meyer and A. S. Foster, *Sci. Adv.*, 2018, **4**, eaar7181.
8 X. Y. Wang, X. Yao, A. Narita and K. Mullen, *Acc. Chem. Res.*, 2019, **52**, 2491–2505.
9 C. Hu, D. Liu, Y. Xiao and L. Dai, *Prog. Nat. Sci.*, 2018, **28**, 121–132.
10 H. B. Wu and X. W. D. Lou, *Sci. Adv.*, 2017, **3**, eaap9252.
11 J. Chen, Y. Zhu and S. Kaskel, *Angew. Chem., Int. Ed. Engl.*, 2021, **60**, 5010–5035.
12 S. De, T. Devic and A. Fateeva, *Dalton Trans.*, 2021, **50**, 1166–1188.
13 F. Figueira and F. A. A. Paz, *C*, 2021, **7**, 47.
14 S. S. Rajasree, X. Li and P. Deria, *Commun. Chem.*, 2021, **4**, 47.
15 X. Zhao, P. Pachfule and A. Thomas, *Chem. Soc. Rev.*, 2021, **50**, 6871–6913.
16 M. Lu, M. Zhang, J. Liu, Y. Chen, J. P. Liao, M. Y. Yang, Y. P. Cai, S. L. Li and Y. Q. Lan, *Angew. Chem., Int. Ed. Engl.*, 2022, **61**, e202200003.
17 Z. Liang, H. Y. Wang, H. Zheng, W. Zhang and R. Cao, *Chem. Soc. Rev.*, 2021, **50**, 2540–2581.
18 S. Huang, K. Chen and T.-T. Li, *Coord. Chem. Rev.*, 2022, **464**, 214563.
19 N. Kobayashi, *Chem. Phys. Lett.*, 1993, **205**, 51–54.
20 T. D. Lash, *J. Porphyrins Phthalocyanines*, 2001, **5**, 267–288.
21 S. Hayashi, M. Tanaka, H. Hayashi, S. Eu, T. Umeyama, Y. Matano, Y. Araki and H. Imahori, *J. Phys. Chem. C*, 2008, **112**, 15576–15585.
22 A. V. Cheprakov and M. A. Filatov, *J. Porphyrins Phthalocyanines*, 2009, **13**, 291–303.
23 N. Ono, H. Yamada and T. Okujima, *Synthesis of Porphyrins Fused with Aromatic Rings*, World Scientific, Singapore, 2010.

24 L. J. K. Boerner, S. Mazumder, M. Pink, J. M. Zaleski and M.-H. Baik, *Chem.–Eur. J.*, 2011, **17**, 14539–14551.
25 A. V. Cheprakov, *The Synthesis of pi-Extended Porphyrins*, World Scientific Publishing, Singapore, 2011.
26 C.-L. Wang, Y.-C. Chang, C.-M. Lan, C.-F. Lo, E. Wei-Guang Diau and C.-Y. Lin, *Energy Environ. Sci.*, 2011, **4**, 1788–1795.
27 J. M. Ball, N. K. S. Davis, J. D. Wilkinson, J. Kirkpatrick, J. Teuscher, R. Gunning, H. L. Anderson and H. J. Snaith, *RSC Adv.*, 2012, **2**, 6846–6853.
28 C. M. Carvalho, T. J. Brocksom and K. T. de Oliveira, *Chem. Soc. Rev.*, 2013, **42**, 3302–3317.
29 V. V. Roznyatovskiy, C. H. Lee and J. L. Sessler, *Chem. Soc. Rev.*, 2013, **42**, 1921–1933.
30 A. Chaudhary, A. Srinivasan and T. K. Chandrashekar, *Handbook of Porphyrin Science*, 2014.
31 H. Yamada, D. Kuzuhara, T. Takahashi, Y. Shimizu, K. Uota, T. Okujima, H. Uno and N. Ono, *Org. Lett.*, 2008, **10**, 2947–2950.
32 N. K. S. Davis, A. L. Thompson and H. L. Anderson, *J. Am. Chem. Soc.*, 2011, **133**, 30–31.
33 J. P. Lewtak and D. T. Gryko, *Chem. Commun.*, 2012, **48**, 10069–10086.
34 D. Mysliwiec, B. Donnio, P. J. Chmielewski, B. Heinrich and M. Stepien, *J. Am. Chem. Soc.*, 2012, **134**, 4822–4833.
35 P. Chen, Y. Fang, K. M. Kadish, J. P. Lewtak, D. Koszelewski, A. Janiga and D. T. Gryko, *Inorg. Chem.*, 2013, **52**, 9532–9538.
36 D. Koszelewski, A. Nowak-Król, M. Drobizhev, C. J. Wilson, J. E. Haley, T. M. Cooper, J. Romiszewski, E. Górecka, H. L. Anderson, A. Rebane and D. T. Gryko, *J. Mater. Chem. C*, 2013, **1**, 2044–2053.
37 Y. Fang, D. Koszelewski, K. M. Kadish and D. T. Gryko, *Chem. Commun.*, 2014, **50**, 8864–8867.
38 N. Fukui, H. Yorimitsu and A. Osuka, *Angew. Chem., Int. Ed. Engl.*, 2015, **54**, 6311–6314.
39 N. Fukui, S. K. Lee, K. Kato, D. Shimizu, T. Tanaka, S. Lee, H. Yorimitsu, D. Kim and A. Osuka, *Chem. Sci.*, 2016, **7**, 4059–4066.
40 N. Fukui and A. Osuka, *Angew. Chem., Int. Ed. Engl.*, 2018, **57**, 6304–6308.
41 R. W. Hooper, A. Zhang, D. Koszelewski, J. P. Lewtak, B. Koszarna, C. J. Levy, D. T. Gryko and M. J. Stillman, *J. Porphyrins Phthalocyanines*, 2018, **22**, 1111–1128.
42 K. Kato, K. Furukawa, T. Mori and A. Osuka, *Chem.–Eur. J.*, 2018, **24**, 572–575.
43 J. R. Reimers, L. E. Hall, M. J. Crossley and N. S. Hush, *J. Phys. Chem. A*, 1999, **103**, 4385–4397.
44 J. N. H. Reek, A. E. Rowan, R. d. Gelder, P. T. Beurskens, M. J. Crossley, S. D. Feyter, F. d. Schryver and R. J. M. Nolte, *Angew. Chem., Int. Ed. Engl.*, 1997, **36**, 361–363.
45 Z. Ou, T. Khoury, Y. Fang, W. Zhu, P. J. Sintic, M. J. Crossley and K. M. Kadish, *Inorg. Chem.*, 2013, **52**, 2474–2483.
46 C. B. Dover, J. K. Gallaher, L. Frazer, P. C. Tapping, A. J. Petty II, M. J. Crossley, J. E. Anthony, T. W. Kee and T. W. Schmidt, *Nat. Chem.*, 2018, **10**, 305–310.
47 M. J. Crossley and L. A. Johnston, *Chem. Commun.*, 2002, 1122–1123.
48 M. J. Crossley and P. L. Burn, *J. Chem. Soc., Chem. Commun.*, 1991, 1569–1571.
49 P. J. Canfield, I. M. Blake, Z. L. Cai, I. J. Luck, E. Krausz, R. Kobayashi, J. R. Reimers and M. J. Crossley, *Nat. Chem.*, 2018, **10**, 615–624.
50 K. P. Birin, A. I. Poddubnaya, I. A. Abdulaeva, Y. G. Gorbunova and A. Y. Tsivadze, *Dyes Pigm.*, 2018, **156**, 243–249.
51 Y. Kashiwagi, K. Ohkubo, J. A. McDonald, I. M. Blake, M. J. Crossley, Y. Araki, O. Ito, H. Imahori and S. Fukuzumi, *Org. Lett.*, 2003, **5**, 2719–2721.
52 H. Hayashi, A. S. Touchy, Y. Kinjo, K. Kurotobi, Y. Toude, S. Ito, H. Saarenpaa, N. V. Tkachenko, H. Lemmetyinen and H. Imahori, *ChemSusChem*, 2013, **6**, 508–517.
53 J. Zhao, J. I. Wong, J. Gao, G. Li, G. Xing, H. Zhang, T. C. Sum, H. Y. Yang, Y. Zhao, S. L. Ake Kjelleberg, W. Huang, S. C. Joachim Loo and Q. Zhang, *RSC Adv.*, 2014, **4**, 17822–17831.
54 J. Guo, Y. Xu, S. Jin, L. Chen, T. Kaji, Y. Honsho, M. A. Addicoat, J. Kim, A. Saeki, H. Ihee, S. Seki, S. Irle, M. Hiramoto, J. Gao and D. Jiang, *Nat. Commun.*, 2013, **4**, 2736.
55 J. Chen, J. Qu, Y. Zhang, Y. Chen, N. Liu and B. Chen, *Tetrahedron*, 2013, **69**, 316–319.
56 J. Velik, V. Baliharova, J. Fink-Gremmels, S. Bull, J. Lamka and L. Skalova, *Res. Vet. Sci.*, 2004, **76**, 95–108.
57 S. R. Brishty, M. J. Hossain, M. U. Khandaker, M. R. I. Faruque, H. Osman and S. M. A. Rahman, *Front. Pharmacol.*, 2021, **12**, 762807.
58 E. Mishra, J. L. Worlinsky, T. M. Gilbert, C. Bruckner and V. Ryzhov, *J. Am. Soc. Mass Spectrom.*, 2012, **23**, 1135–1146.
59 M.-S. Liao, M.-J. Huang and J. D. Watts, *J. Phys. Chem. A*, 2010, **114**, 9554–9569.
60 E. Y. Kaigorodova, G. M. Mamardashvili, O. R. Simonova, N. V. Chizhova and N. Z. Mamardashvili, *J. Coord. Chem.*, 2021, **74**, 2443–2462.
61 R. Deshpande, L. Jiang, G. Schmidt, J. Rakovan, X. Wang, K. Wheeler and H. Wang, *Org. Lett.*, 2009, **11**, 4251–4253.
62 L. Jiang, J. T. Engle, L. Sirk, C. S. Hartley, C. J. Ziegler and H. Wang, *Org. Lett.*, 2011, **13**, 3020–3023.
63 L. Jiang, R. A. Zaenglein, J. T. Engle, C. Mittal, C. S. Hartley, C. J. Ziegler and H. Wang, *Chem. Commun.*, 2012, **48**, 6927–6929.
64 L. Jiang, J. T. Engle, R. A. Zaenglein, A. Matus, C. J. Ziegler, H. Wang and M. J. Stillman, *Chem.–Eur. J.*, 2014, **20**, 13865–13870.
65 Y. Hu, M. B. Thomas, W. A. Webre, A. Moss, R. G. W. Jinadasa, V. N. Nesterov, F. D'Souza and H. Wang, *Angew. Chem., Int. Ed.*, 2020, **132**, 20250–20257.
66 S. A. Vinogradov and D. F. Wilson, *In Designing Dendrimers*, Wiley, New York, 2012.
67 M. Quaranta, S. M. Borisov and I. Klimant, *Bioanalytical Reviews*, 2012, **4**, 115–157.
68 D. B. Papkovsky and R. I. Dmitriev, *Chem. Soc. Rev.*, 2013, **42**, 8700–8732.
69 M. Pawlicki, H. A. Collins, R. G. Denning and H. L. Anderson, *Angew. Chem., Int. Ed.*, 2009, **48**, 3244–3266.

70 K. S. Kim, J. M. Lim, A. Osuka and D. Kim, *J. Photochem. Photobiol., C*, 2008, **9**, 13–28.
71 C. Y. Liu, M. Deb, A. S. Sadhu, R. Karmakar, P. T. Huang, Y. N. Lin, C. S. Chu, B. N. Pal, S. H. Chang and S. Biring, *Sensors*, 2021, **21**, 6940.
72 Y. Zhao, X. Geng, X. Shi, Y. Guo, Y. Sun, L. Qu and Z. Li, *J. Mater. Chem. C*, 2021, **9**, 4300–4306.
73 P. J. Hay and W. R. Wadt, *J. Chem. Phys.*, 1985, **82**, 270–283.
74 W. R. Wadt, P. J. Hay and J. Chem, *Phys*, 1985, **82**, 284–298.
75 P. J. Hay and W. R. Wadt, *J. Chem. Phys.*, 1985, **82**, 299–310.
76 C. Latouche, D. Skouteris, F. Palazzetti and J. Barone, *J. Chem. Theory Comput.*, 2015, **11**, 3281–3289.
77 A. Jana, L. McKenzie, A. B. Wragg, M. Ishida, J. P. Hill, J. A. Weinstein, E. Baggaley and M. D. Ward, *Chem.–Eur. J.*, 2016, **22**, 4164.
78 M. J. Gouterman, *The Porphyrins*, Academic Press, New York, 1978.
79 M. J. Gouterman, *Mol. Spectrosc.*, 1961, **6**, 138–163.
80 S. Montanaro, D. G. Congrave, M. K. Etherington and I. A. Wright, *J. Mater. Chem. C*, 2019, **7**, 12886–12890.
81 K. Jana and J. N. Moorthy, *New J. Chem.*, 2022, **46**, 1416–1422.
82 K. Baumgartner, M. Hoffmann, F. Rominger, S. M. Elbert, A. Dreuw and M. Mastalerz, *J. Org. Chem.*, 2020, **85**, 15256–15272.
83 K. M. Kadish, *Prog. Inorg. Chem.*, 1986, **34**, 435–605.
84 D. M. Guldi, *Chem. Soc. Rev.*, 2002, **31**, 22–36.
85 C. B. KC and F. D'Souza, *Coord. Chem. Rev.*, 2016, **322**, 104–141.
86 F. D'Souza, O. Ito and O. Coord, *Chem. Rev.*, 2005, **249**, 1410–1422.
87 D. Rehm and A. Weller, *Isr. J. Chem.*, 1970, **10**, 259–271.
88 R. A. Marcus, *Angew. Chem., Int. Ed. Engl.*, 1993, **32**, 1111–1121.
89 C. O. Obondi, G. N. Lim, B. Churchill, P. K. Poddutoori, A. vaa der Est and F. D'Souza, *Nanoscale*, 2016, **8**, 8333–8345.